Association mapping of inflammatory bowel disease loci to single variant resolution

Hailiang Huang[1,2]*§, Ming Fang[3,4]*, Luke Jostins[5,6]*, Maša Umićević Mirkov[7], Gabrielle Boucher[8], Carl A Anderson[7], Vibeke Andersen[9,10], Isabelle Cleynen[11], Adrian Cortes[5], François Crins[3,4], Mauro D'Amato[12,13], Valérie Deffontaine[3,4], Julia Dimitrieva[3,4], Elisa Docampo[3,4], Mahmoud Elansary[3,4], Kyle Kai-How Farh[1,2,14], Andre Franke[15], Ann-Stephan Gori[3,4], Philippe Goyette[8], Jonas Halfvarson[16], Talin Haritunians[17], Jo Knight[18], Ian C Lawrance[19,20], Charlie W Lees[21], Edouard Louis[22], Rob Mariman[3,4], Theo Meuwissen[3,4], Myriam Mni[3,4], Yukihide Momozawa[3,4,23], Miles Parkes[24], Sarah L Spain[25,26], Emilie Théâtre[3,4], Gosia Trynka[7], Jack Satsangi[21], Suzanne van Sommeren[27], Severine Vermeire[11,28], Ramnik J Xavier[2,29], International IBD Genetics Consortium†, Rinse K Weersma[27], Richard H Duerr[30,31], Christopher G Mathew[25,32], John D Rioux[8,33], Dermot PB McGovern[17], Judy H Cho[34], Michel Georges[3,4]§, Mark J Daly[1,2]§, Jeffrey C Barrett[7]§

[1]Analytic and Translational Genetics Unit, Massachusetts General Hospital, Harvard Medical School, Boston, Massachusetts, USA. [2]Broad Institute of MIT and Harvard, Cambridge, Massachusetts, USA. [3]Unit of Animal Genomics, Groupe Interdisciplinaire de Génoprotéomique Appliquée (GIGA-R) Research Center, University of Liège, Liège, Belgium. [4]Faculty of Veterinary Medicine, University of Liège, Liège, Belgium. [5]Wellcome Trust Centre for Human Genetics, University of Oxford, Headington, UK. [6]Christ Church, University of Oxford, St Aldates, UK. [7]Wellcome Trust Sanger Institute, Hinxton (Cambridge), UK. [8]Research Center, Montreal Heart Institute, Montréal, Québec, Canada. [9]Medical Department, Viborg Regional Hospital, Viborg, Denmark. [10]Organ Center, Hospital of Southern Jutland Aabenraa, Aabenraa, Denmark. [11]Department of Clinical and experimental medicine, Translational Research in GastroIntestinal Disorders (TARGID), Katholieke Universiteit (KU) Leuven, Leuven, Belgium. [12]Department of Biosciences and Nutrition, Karolinska Institutet, Stockholm, Sweden. [13]BioCruces Health Research Institute and IKERBASQUE, Basque Foundation for Science, Bilbao, Spain. [14]Illumina, San Diego, California, USA. [15]Institute of Clinical Molecular Biology, Christian-Albrechts-University of Kiel, Kiel, Germany. [16]Department of Gastroenterology, Faculty of Medicine and Health, Örebro University, Örebro, Sweden. [17]F.Widjaja Foundation Inflammatory Bowel and Immunobiology Research Institute, Cedars-Sinai Medical Center, Los Angeles, California, USA. [18]Campbell Family Mental Health Research Institute, Centre for Addiction and Mental Health, Toronto, Ontario, Canada. [19]Centre for Inflammatory Bowel Diseases, Saint John of God Hospital, Subiaco, WA, Australia. [20]Harry Perkins Institute for Medical Research, School of Medicine and Pharmacology, University of Western Australia, Murdoch, WA, Australia. [21]Gastrointestinal Unit, Wester General Hospital University of Edinburgh, Edinburgh, UK. [22]Division of Gastroenterology, Centre Hospitalier Universitaire (CHU) de Liège, Liège, Belgium. [23]Laboratory for Genotyping Development, Center for Integrative Medical Sciences, RIKEN, Yokohama, Japan. [24]Inflammatory Bowel Disease Research Group, Addenbrooke's Hospital, Cambridge, UK. [25]Department of Medical and Molecular Genetics, King's College London, London, UK. [26]Centre for Therapeutic Target Validation, Wellcome Trust Genome Campus, Hinxton (Cambridge), UK. [27]Department of Gastroenterology and Hepatology, University Medical Center Groningen, Groningen, The Netherlands. [28]Division of Gastroenterology, University Hospital Gasthuisberg, Leuven, Belgium. [29]Gastroenterology Unit, Massachusetts General Hospital, Harvard Medical School, Boston, Massachusetts, USA. [30]Division of Gastroenterology, Hepatology and Nutrition, Department of Medicine, University of Pittsburgh School of Medicine, Pittsburgh, Pennsylvania, USA. [31]Department of Human Genetics, University of Pittsburgh Graduate School of Public Health, Pittsburgh, Pennsylvania, USA. [32]Sydney Brenner Institute for Molecular Bioscience, University of the Witwatersrand, Johannesburg, South Africa . [33]Faculté de Médecine, Université de Montréal, Montréal, Québec, Canada. [34]Department of Genetics, Yale School of Medicine, New Haven, Connecticut, USA.

*These authors contributed equally to this work.
§These authors contributed equally to this work (corresponding authors).
†A full list of members and affiliations appears in the Supplementary Information.

Summary

Inflammatory bowel disease (IBD) is a chronic gastrointestinal inflammatory disorder that affects millions worldwide. Genome-wide association studies (GWAS) have identified 200 IBD-associated loci, but few have been conclusively resolved to specific functional variants. Here we report fine-mapping of 94 IBD loci using high-density genotyping in 67,852 individuals. Of the 139 independent associations identified in these regions, 18 were pinpointed to a single causal variant with >95% certainty, and an additional 27 associations to a single variant with >50% certainty. These 45 variants are significantly enriched for protein-coding changes (n=13), direct disruption of transcription factor binding sites (n=3) and tissue specific epigenetic marks (n=10), with the latter category showing enrichment in specific immune cells among associations stronger in CD and gut mucosa among associations stronger in UC. The results of this study suggest that high-resolution, fine-mapping in large samples can convert many GWAS discoveries into statistically convincing causal variants, providing a powerful substrate for experimental elucidation of disease mechanisms.

Inflammatory bowel disease (IBD) is a chronic, debilitating disorder of the gastrointestinal tract with peak onset in adolescence and early adulthood. More than 1.4 million people are affected in the USA alone[1], with an estimated direct healthcare cost of $6.3 billion/year. IBD affects millions worldwide with a rising prevalence, particularly in pediatric and non-European ancestry populations[2]. IBD is comprised of two etiologically related subtypes, ulcerative colitis (UC) and Crohn's disease (CD), which have distinct presentations and treatment courses. To date, 200 genomic loci have been associated with IBD[3,4], but only a handful have been conclusively ascribed to a specific causal variant with direct insight into the underlying disease biology. This scenario is common to all genetically complex diseases, where the pace of identifying associated loci outstrips that of defining specific molecular mechanisms and extracting biological insight from each association.

The widespread correlation structure of the human genome (known as linkage disequilibrium, or LD) often results in similar evidence for association among many nearby variants. However, unless LD is perfect ($r^2 = 1$), it is possible, with sufficiently large sample size, to statistically resolve causal variants from neighbors even at high levels of correlation (Extended Data Figure 1 and van de Bunt *et al.*[5]). Novel statistical approaches applied to very large datasets have begun to address this problem[6] but also require that the highly correlated variants are directly genotyped or imputed with certainty. Truly high-resolution mapping data, when combined with increasingly sophisticated and comprehensive public databases annotating the putative protein-coding and regulatory function of DNA variants, are likely to reveal novel insights into disease pathogenesis[7-9] and the mechanistic involvement of disease-associated variants.

90

91 **Genetic architecture of IBD associated loci**

92 As part of a large collaborative effort led by the International IBD Genetics Consortium
93 (IIBDGC), 67,852 study subjects of European ancestry, including 33,595 IBD (18,967
94 CD and 14,628 UC) and 34,257 healthy controls were genotyped using the Illumina™
95 (San Diego, CA, USA) Immunochip. This custom genotyping array was designed to
96 include all known variants from European individuals in the February 2010 release of the
97 1000 Genomes Project[10,11] in 186 high-density regions known to be associated to one or
98 more of 12 immune-mediated diseases[12]. We evaluated ninety-seven of these regions
99 previously associated with IBD[3] and containing one or more associated variants ($p < 10^{-6}$)
100 in this data set. The major histocompatibility complex was excluded from these analyses
101 as fine-mapping has been reported elsewhere[13]. Because fine-mapping uses subtle
102 differences in strength of association between tightly correlated variants to infer which is
103 most likely to be causal, it is particularly sensitive to data quality. We therefore
104 performed stringent quality control (QC) to remove genotyping errors and batch effects,
105 including manual cluster plot inspection for 905 variants (Methods). After QC, we
106 imputed this dataset using the 1000 Genomes reference panel (December 2013,
107 downloaded from IMPUTE2[14,15] website) to fill in missing variants or genotype data
108 dropped in chip design or QC (Figure 1a).

109 We applied three complementary Bayesian fine-mapping methods that used
110 different priors and model selection strategies both to identify independent association
111 signals within a region (Supplementary Methods), and to assign a posterior probability of
112 causality to each variant (Figure 1a). For each independent association signal, we sorted

113 all variants by the posterior probability of association, and added variants to the 'credible
114 set' of associated variants until the sum of their posterior probability exceeded 95% –
115 that is, the credible set contains the minimum list of DNA variants that are >95% likely to
116 contain the causal variant (Figure 1b). These sets ranged in size from one to > 400
117 variants. We merged these results (Methods) and subsequently focused (Figure 1a) only
118 on signals where an overlapping credible set of variants was identified by at least two of
119 the three methods and all variants were either directly genotyped or well imputed
120 (Methods). Fluorescent signal intensity cluster plots were manually reviewed for all
121 variants in credible sets with ten or fewer variants, and a second round of imputation and
122 analysis was performed if any genotypes were removed based on this review.
123 In 3 out of 97 regions, a consistent credible set could not be identified; when
124 multiple independent effects exist in a region with several highly correlated signals,
125 multiple distinct fine-mapping solutions may not be distinguishable (Supplementary
126 Notes). Sixty-eight of the remaining 94 regions contain a single credible set, while 26
127 harbored two or more independent association signals, for a total of 139 independent
128 associations defined across the 94 regions (Figure 2a). Only *IL23R* and *NOD2* (both
129 previously established to contain multiple associated protein-coding variants[16]), contain
130 more than three independent signals. Consistent with previous reports[3], the vast majority
131 of signals are associated with both CD and UC. However, many of these have
132 significantly stronger association with one subtype than the other. For the purposes of
133 enrichment analyses below, we compare 79 signals that are more strongly associated with
134 CD to 23 signals that are more strongly associated with UC (the remaining 37 are equally
135 associated with both subtypes) ("list of credible sets" sheet, Supplementary Table 1).

136 Using a restricted maximum likelihood mixed model approach[17], we evaluated the
137 proportion of total variance in disease risk attributed to these 94 regions and how much of
138 that is explained by the 139 specific associations. We estimated that 25% of CD risk was
139 explained by the specific associations described here, out of a total of 28% explained by
140 these loci (the corresponding numbers for UC are 17% out of 22%). This indicates that
141 our credible sets capture most of the IBD genetic risk at these loci. The single strongest
142 signals in each region contribute 76% of this variance explained and the remaining
143 associations contribute 24% (Extended Data Figure 2b), highlighting the importance of
144 secondary and tertiary associations in the articulation of GWAS results[13,18].
145
146 **Associations mapped to a single variant**
147 For 18 independent signals, the 95% credible set consisted of a single variant (hereafter
148 referred to as 'single variant credible sets') and for 24 others, the credible set consisted of
149 two to five variants (Figure 2b). The single variant credible sets included five previously
150 reported coding variants: three in *NOD2* (fs1007insC, R702W, G908R), a rare protective
151 allele in *IL23R* (V362I) and a splice variant in *CARD9* (c.IVS11+1G>C) [16,19]. The
152 remaining single variant credible sets were comprised of three missense variants (I170V
153 in *SMAD3*, I923V in *IFIH1* and N289S in *NOD2*), four intronic variants (in *IL2RA*,
154 *LRRK2*, *NOD2* and *RTEL1*/*TNFRSF6B*) and six intergenic variants (located 3.7kb
155 downstream of *GPR35*; 3.9kb upstream of *PRDM1*; within a EP300 binding site 39.9 kb
156 upstream of *IKZF1*; 500 bp before the transcription start site of *JAK2*; 9.4kb upstream of
157 *NKX2-3;* and 3.5kb downstream from *HNF4A*) (Table 1). A customizable browser
158 (https://atgu.shinyapps.io/Finemapping) enabling review of the detailed fine-mapping

159 results in each region along with all annotations discussed below has been prepared. Of
160 note, while physical proximity does not guarantee functional relevance, the credible set of
161 variants for 29 associated loci now resides within 50 kb of only a single gene – improved
162 from only 3 so refined using an earlier HapMap-based definition. Using the same
163 definitions, the total number of potential candidate genes was reduced from 669 to 331.
164 Examples of IBD candidate genes clearly prioritized in our data are described in the
165 Supplementary Box.
166
167 **Sequence-level consequences of associated variants – protein coding variation**
168 We first annotated the possible functional consequences of the IBD variants by their
169 effect on the amino acid sequences of proteins. Thirteen out of 45 variants that have
170 >50% posterior probability are non-synonymous (Table 1 and Figure 2c), an 18-fold
171 enrichment (p-value=$2x10^{-13}$, Fisher's exact test) relative to randomly drawn variants in
172 our regions. By contrast, only one variant with >50% probability is synonymous
173 (p=0.42). All common coding variants previously reported to affect IBD risk are
174 included in a 95% credible set including: *IL23R* (R381Q, V362I and G149R); *CARD9*
175 (c.IVS11+1G>C and S12N); *NOD2* (S431L, R702W, V793M, N852S and G908R,
176 fs1007insC); *ATG16L1* (T300A); *PTPN22* (R620W); and *FUT2* (W154X). While this
177 enrichment of coding variation (Figure 3a) provides assurance about the accuracy of our
178 approach, it does not suggest that 30% of all associations are caused by coding variants;
179 rather, it is almost certainly the case that associated coding variants have stronger effect
180 sizes, making them more amenable to fine mapping.
181

182 **Sequence-level consequences of associated variants – non-coding variation**

183 We next examined the best understood non-coding aspect of DNA sequence: conserved
184 nucleotides in high confidence binding site motifs of 84 transcription factor (TF)
185 families[20] (Methods). There was a significant positive correlation between TF motif
186 disruption and IBD association posterior probability (p-value=0.006, binomial
187 regression) (Figure 3a), including three variants with >50% probability (two >95%). In
188 the *RTEL1/TNFRSF6B* region, rs6062496 region is predicted to disrupt a TF binding site
189 (TFBS) for EBF1 and overlaps DNaseI hypersensitivity clusters. EBF1 is a TF involved
190 in the maintenance of B cell identity and prevention of alternative fates in committed
191 cells[21]. The second example, rs74465132, is a low frequency (3.6%) protective variant
192 that creates a binding site for EP300 less than 40kbp upstream of *IKZF1* (zinc-finger
193 DNA binding protein). The third notable example of TFBS disruption, although not in a
194 single variant credible set, is detailed in the Supplementary Box for the association at
195 *SMAD3*.

196 Recent studies have shown that trait associated variants are enriched for
197 epigenetic marks highlighting cell type specific regulatory regions [22,23]. We compared our
198 credible sets with ChIPseq peaks corresponding to chromatin immunoprecipitation with
199 H3K4me1, H3K4me3 and H3K27ac in 120 adult and fetal tissues, assayed by the NIH
200 Roadmap Epigenomics Mapping Consortium[24] (Figure 3b). Using a threshold of
201 $p=1.3x10^{-4}$ (0.05 corrected for 360 tests), we observed significant enrichment of
202 H3K4me1 in 6 immune cell types and for H3K27ac in 3 gastrointestinal (GI) samples
203 (sigmoid colon and colonic and rectal mucosa) (Figure 3b and Supplementary Table 2).
204 Furthermore, the subset of signals that are more strongly associated with CD overlap

205 more with immune cell chromatin peaks, whereas UC signals overlap more with GI
206 chromatin peaks (Supplementary Table 2).
207 These three chromatin marks are correlated both within tissues (we observe
208 additional signal in other marks in the tissues described above) and across related tissues.
209 We therefore defined a set of "core immune peaks" for H3K4me1 and "core GI peaks"
210 for H3K27ac as the set of overlapping peaks in all enriched immune cell and GI tissue
211 types, respectively. These two tracks (immune-K4me1 and gut-K27ac) are independently
212 significant and capture the observed enrichment compared to "control peaks" made up of
213 the same number of ChIPseq peaks across our 94 regions in non-immune and non-GI
214 tissues (Figure 3c,d). These two tracks summarize our epigenetic-GWAS overlap signal,
215 and the combined excess over the baseline suggests that a substantial number of regions,
216 particularly those not mapped to coding variants, may ultimately be explained by
217 functional variation in recognizable enhancer/promoter elements.
218
219 **Overlap of IBD credible sets with expression QTLs**
220 Variants that change enhancer or promoter activity might precipitate changes in gene
221 expression, and baseline expression of many genes has been found to be regulated by
222 genetic variation[25-27]. Indeed, these so-called expression quantitative trait loci (eQTLs)
223 have been suggested to underlie a large proportion of GWAS associations [25,28]. We
224 therefore searched for variants that are both in an IBD associated credible set with 50 or
225 fewer variants and the most significantly associated eQTL variant for a gene in the
226 GODOT study[29] of peripheral blood mononuclear cells (PBMC) from 2,752 twins.
227 Sixty-eight of the 76 regions with signals fine-mapped to < 50 variants harbor at least one

228 significant eQTL (defined as influencing expression of a gene within 1 Mb of the region
229 with a p-value < 10^{-5}). Despite this apparent abundance of eQTLs in fine-mapped
230 regions, only 3 credible sets overlap eQTLs, compared with 3.7 expected by chance
231 (Methods). Data from a more recent independent study (Westra *et al.*)[30] using PBMCs
232 from 8,086 individuals did not yield a substantively different outcome, demonstrating a
233 modest but non-significant enrichment (8 observed overlaps, 4.2 expected by chance,
234 p=0.07). Using a more lenient definition of overlap which requires the lead eQTL variant
235 to be in LD ($R^2 > 0.4$) with an IBD credible set variant increased the number of potential
236 overlaps but again these numbers were not greater than chance expectation (GODOT:
237 observed 14, expected 12.2; Westra *et al.*: observed 11, expected 9.1).
238 As PBMCs are a heterogeneous collection of immune cell populations, cell type-
239 specific signals, or signals corresponding to genes expressed most prominently in non-
240 immune tissues, may be missed. We therefore tested the enrichment of eQTLs that
241 overlap credible sets in 5 primary T cell populations (CD4+, CD8+, CD19+, CD14+ and
242 CD15+), platelets, and 3 distinct intestinal locations (rectum, colon and ileum) isolated
243 from 350 healthy individuals (ULg dataset, Methods). We observed a significant
244 enrichment of credible SNP/eQTL overlaps in CD4+ cells and ileum (Extended Table 1):
245 3 and 2 credible sets overlapped eQTLs, respectively, compared to 0.4 and 0.3 expected
246 by chance (p-value=0.007 and 0.025). An enrichment was also observed for the naïve
247 CD14+ cells from another study[31] (Knight dataset, Extended Data Table 1): eight
248 overlaps observed compared to 2.7 expected by chance (p-value=0.005). We did not
249 observe enrichment of overlaps in stimulated (with interferon or lipopolysaccharide)
250 CD14+ cells from the same source (Extended Data Table 1).

251 To more deeply investigate eQTL overlaps we applied two colocalization
252 approaches (one based on permutations, one Bayesian, Methods) to eQTL datasets where
253 primary genotype and expression data were available (ULg dataset). We confirmed
254 greater than expected overlap with eQTLs in CD4+ and ileum described above (Figure 4
255 and Extended Data Table 1). The number of colocalizations in other purified cell
256 types/tissues was largely indistinguishable from what we expect under the null using
257 either method, except for moderate enrichment in rectum (4 observed and 1.4 expected,
258 p=0.039) and colon (3 observed and 0.8 expected, p=0.04). Of these robust
259 colocalizations, only two correspond to an IBD variant with causal probability > 50%
260 (Table 1 and Extended Data Figure 3a).
261
262 **Discussion**
263 We have performed fine-mapping of 94 previously reported genetic risk loci for IBD.
264 Rigorous quality control followed by a integration of three novel fine-mapping methods
265 was employed to generate a list of genetic variants accounting for 139 independent
266 associations across these loci. These associations account for more than 80% of the total
267 variance explained by these loci. Our results substantially improve on previous fine-
268 mapping efforts using a preset LD threshold (e.g. $r^2 > 0.6$[32]) (Figure 5) by formally
269 modeling the posterior probability of association of every variant. Much of this
270 resolution derives from the very large sample size we employed, because the number of
271 variants in a credible set significantly decreases with increasing test statistics (p-value =
272 0.0069, Extended Data Figure 4). For example, at 10% allele frequency, 31% of signals

273 are fine-mapped to ≤ 5 variants – this improves to 53% if the sample size were to double
274 again.

275 Additionally, the high-density of genotyping also aids in improved resolution.
276 For instance, the primary association at IL2RA has now been mapped to a single variant
277 associated with CD, rs61839660. This variant was not present in the Hapmap 3 reference
278 panel and was therefore not reported in earlier studies[3,33] (nearby tagging variants,
279 rs12722489 and rs12722515, were reported instead). Imputation using the 1000 genomes
280 reference panel and the largest assembled GWAS dataset[3] did not separate rs61839660
281 from its neighbors (unpublished results), due to the loss of information in imputation
282 using the limited reference. Only direct genotyping, available in the immunochip high-
283 density regions, permitted the conclusive identification of this as the causal variant.

284 Accurate fine-mapping should, in many instances, ultimately point to the same
285 variant across diseases in shared loci. Among our single-variant credible sets, we fine-
286 mapped a UC association to a rare missense variant (I923V) in *IFIH1*, which is also
287 associated with type 1 diabetes (T1D)[34] with an opposite direction of effect
288 (Supplementary Box). The intronic variant noted above (rs61839660, AF=9%) in *IL2RA*
289 was also similarly associated with T1D, again with a discordant directional effect[35]
290 (Supplementary Box). Simultaneous high-resolution fine-mapping in multiple diseases
291 should therefore better clarify both shared and distinct biology.

292 High-resolution fine-mapping demonstrates that causal variants are significantly
293 enriched for variants that alter protein coding variants or disrupt transcription factor
294 binding motifs. Enrichment was also observed in H3K4me1 marks in immune related
295 cell types and H3K27ac marks in sigmoid colon and rectal mucosal tissues – with CD

296 loci demonstrating a stronger immune signature and UC loci more enriched for gut
297 tissues. By contrast, overall enrichment of eQTLs is quite modest compared with prior
298 reports and not seen in excess of chance in our well-refined credible sets. This result
299 underscores not only the importance of the high-resolution mapping but also the careful
300 incorporation of the high background rate of eQTLs. It is worth noting that evaluating
301 the overlap between two distinct mapping results is fundamentally different than
302 comparing genetic mapping results to fixed genomic features, and depends on both
303 mappings being well-resolved. While these data strongly challenge the paradigm that
304 easily surveyed baseline eQTLs explain a large proportion of non-coding GWAS signals,
305 the modest excesses observed in smaller but cell-specific data sets suggest that much
306 larger tissue or cell-specific studies (and under the correct stimuli or developmental time
307 points) will resolve the contribution of eQTLs to GWAS hits.

308 Resolving multiple independent associations may often help target the causal gene
309 more precisely. For example, the *SMAD3* locus hosts a non-synonymous variant and a
310 variant disrupting the conserved transcription factor binding site (also overlapping the
311 H3K27ac marker in gut tissues), unambiguously articulating a role in disease and
312 providing an allelic series for further experimental inquiry. Similarly, the *TYK2* locus has
313 been mapped to a non-synonymous variant and a variant disrupting a conserved
314 transcription factor binding site (Extended Data Figure 5).

315 One-hundred and sixteen associations have been fine-mapped to ≤ 50 variants.
316 Among them, 27 associations contain coding variants, 20 contain variants disrupting
317 transcription factor binding motifs, and 45 are within histone H3K4me1 or H3K27ac
318 marked DNA regions. However, 40 non-coding associations were not mapped to any

319 known function (Extended Data Figure 3b) despite extensive efforts to integrate with all
320 available annotation, epigenetic and eQTL data.

321 The best-resolved associations - 45 variants having >50% posterior probabilities
322 for being causal (Table 1) – are similarly significantly enriched for variants with known
323 or presumed function from genome annotation. Of these, 13 variants cause non-
324 synonymous change in amino acids, 3 disrupt a conserved TF binding motif, 10 are
325 within histone H3K4me1 or H3K27ac marked DNA regions in disease-relevant tissues,
326 and 2 co-localize with a significant cis-eQTL (Extended Data Figure 3a).

327 This analysis leaves, however, 21 non-coding variants, all of which have
328 extremely high probabilities to be causal (5 are in the >95% list), that are not located
329 within known motifs, annotated elements, nor in any experimentally determined ChIPseq
330 peaks or eQTL credible sets yet discovered. While we have identified a statistically
331 compelling set of genuine associations (often intronic or within 10 kb of strong candidate
332 genes), we can make little inference about function. For example, the single variant
333 credible set only 500 bp from the transcription start site of JAK2 has no annotation,
334 eQTL or ChIPseq peak of note. This underscores the incompleteness of our knowledge
335 regarding the function of non-coding DNA and its role in disease. That the majority of
336 the best refined non-coding associations have no available annotation is perhaps sobering
337 with respect to how well we may be able to currently interpret non-coding variation in
338 medical sequencing efforts. It does suggest, however, that detailed fine-mapping of
339 GWAS signals down to single variants, combined with emerging high-throughput
340 genome-editing methodology, may be among the most effective ways to advance to a
341 greater understanding of the biology of the non-coding genome.

342 **References**

343 1. Kappelman, M. D. *et al.* Direct health care costs of Crohn's disease and ulcerative
344 colitis in US children and adults. *Gastroenterology* **135,** 1907–1913 (2008).
345 2. Molodecky, N. A. *et al.* Increasing incidence and prevalence of the inflammatory
346 bowel diseases with time, based on systematic review. *Gastroenterology* **142,** 46–
347 54.e42– quiz e30 (2012).
348 3. Jostins, L. *et al.* Host–microbe interactions have shaped the genetic architecture of
349 inflammatory bowel disease. *Nature* **491,** 119–124 (2012).
350 4. Liu, J. Z. *et al.* Association analyses identify 38 susceptibility loci for
351 inflammatory bowel disease and highlight shared genetic risk across populations.
352 *Nat Genet* (2015). doi:10.1038/ng.3359
353 5. van de Bunt, M. *et al.* Evaluating the Performance of Fine-Mapping Strategies at
354 Common Variant GWAS Loci. *PLoS Genet* **11,** e1005535 (2015).
355 6. Maller, J. B. *et al.* Bayesian refinement of association signals for 14 loci in 3
356 common diseases. *Nat Genet* **44,** 1294–1301 (2012).
357 7. Yang, J. *et al.* FTO genotype is associated with phenotypic variability of body
358 mass index. *Nature* **490,** 267–272 (2012).
359 8. International Multiple Sclerosis Genetics Consortium (IMSGC) *et al.* Analysis of
360 immune-related loci identifies 48 new susceptibility variants for multiple sclerosis.
361 *Nat Genet* **45,** 1353–1360 (2013).
362 9. Onengut-Gumuscu, S. *et al.* Fine mapping of type 1 diabetes susceptibility loci and
363 evidence for colocalization of causal variants with lymphoid gene enhancers. *Nat*
364 *Genet* **47,** 381–386 (2015).
365 10. 1000 Genomes Project Consortium *et al.* An integrated map of genetic variation
366 from 1,092 human genomes. *Nature* **491,** 56–65 (2012).
367 11. 1000 Genomes Project Consortium. A map of human genome variation from
368 population-scale sequencing. *Nature* **467,** 1061–1073 (2010).
369 12. Jostins, L. Using Next-Generation Genomic Datasets In Disease Association. (The
370 University of Cambridge, 2012).
371 13. Goyette, P. *et al.* High-density mapping of the MHC identifies a shared role for
372 HLA-DRB1*01:03 in inflammatory bowel diseases and heterozygous advantage in
373 ulcerative colitis. *Nat Genet* (2015). doi:10.1038/ng.3176
374 14. Howie, B. N., Donnelly, P. & Marchini, J. A flexible and accurate genotype
375 imputation method for the next generation of genome-wide association studies.
376 *PLoS Genet* **5,** e1000529 (2009).
377 15. Howie, B., Marchini, J. & Stephens, M. Genotype imputation with thousands of
378 genomes. *G3 (Bethesda)* **1,** 457–470 (2011).
379 16. Rivas, M. A. *et al.* Deep resequencing of GWAS loci identifies independent rare
380 variants associated with inflammatory bowel disease. *Nat Genet* **43,** 1066–1073
381 (2011).
382 17. Yang, J. *et al.* Genome partitioning of genetic variation for complex traits using
383 common SNPs. *Nat Genet* **43,** 519–525 (2011).
384 18. Huang, H., Chanda, P., Alonso, A., Bader, J. S. & Arking, D. E. Gene-based tests
385 of association. *PLoS Genet* **7,** e1002177 (2011).
386 19. Momozawa, Y. *et al.* Resequencing of positional candidates identifies low

387 frequency IL23R coding variants protecting against inflammatory bowel disease.
388 *Nat Genet* **43,** 43–47 (2011).
389 20. Kheradpour, P. & Kellis, M. Systematic discovery and characterization of
390 regulatory motifs in ENCODE TF binding experiments. *Nucleic Acids Res* **42,**
391 2976–2987 (2014).
392 21. Nechanitzky, R. *et al.* Transcription factor EBF1 is essential for the maintenance
393 of B cell identity and prevention of alternative fates in committed cells. *Nat.*
394 *Immunol.* **14,** 867–875 (2013).
395 22. Trynka, G. *et al.* Chromatin marks identify critical cell types for fine mapping
396 complex trait variants. *Nat Genet* **45,** 124–130 (2013).
397 23. Farh, K. K.-H. *et al.* Genetic and epigenetic fine mapping of causal autoimmune
398 disease variants. *Nature* **518,** 337–343 (2015).
399 24. Bernstein, B. E. *et al.* The NIH Roadmap Epigenomics Mapping Consortium. *Nat*
400 *Biotechnol* **28,** 1045–1048 (2010).
401 25. Nica, A. C. *et al.* Candidate causal regulatory effects by integration of expression
402 QTLs with complex trait genetic associations. *PLoS Genet* **6,** e1000895 (2010).
403 26. Lappalainen, T. *et al.* Transcriptome and genome sequencing uncovers functional
404 variation in humans. *Nature* **501,** 506–511 (2013).
405 27. Wallace, C. *et al.* Statistical colocalization of monocyte gene expression and
406 genetic risk variants for type 1 diabetes. *Human Molecular Genetics* **21,** 2815–
407 2824 (2012).
408 28. Trynka, G. *et al.* Dense genotyping identifies and localizes multiple common and
409 rare variant association signals in celiac disease. *Nat Genet* **43,** 1193–1201 (2011).
410 29. Grundberg, E. *et al.* Mapping cis- and trans-regulatory effects across multiple
411 tissues in twins. *Nat Genet* **44,** 1084–1089 (2012).
412 30. Westra, H.-J. *et al.* Systematic identification of trans eQTLs as putative drivers of
413 known disease associations. *Nat Genet* **45,** 1238–1243 (2013).
414 31. Fairfax, B. P. *et al.* Innate immune activity conditions the effect of regulatory
415 variants upon monocyte gene expression. *Science (New York, NY)* **343,** 1246949–+
416 (2014).
417 32. Schizophrenia Working Group of the Psychiatric Genomics Consortium.
418 Biological insights from 108 schizophrenia-associated genetic loci. *Nature* **511,**
419 421–427 (2014).
420 33. Franke, A. *et al.* Genome-wide meta-analysis increases to 71 the number of
421 confirmed Crohn's disease susceptibility loci. *Nat Genet* **42,** 1118–1125 (2010).
422 34. Nejentsev, S., Walker, N., Riches, D., Egholm, M. & Todd, J. A. Rare variants of
423 IFIH1, a gene implicated in antiviral responses, protect against type 1 diabetes.
424 *Science (New York, NY)* **324,** 387–389 (2009).
425 35. Huang, J., Ellinghaus, D., Franke, A., Howie, B. & Li, Y. 1000 Genomes-based
426 imputation identifies novel and refined associations for the Wellcome Trust Case
427 Control Consortium phase 1 Data. *Eur. J. Hum. Genet.* **20,** 801–805 (2012).
428 36. Roadmap Epigenomics Consortium. Integrative analysis of 111 reference human
429 epigenomes. *Nature* **518,** 317–330 (2015).

Supplementary Information is available in the online version of the paper.

Acknowledgements M.J.D. and R.J.X. acknowledge grant supports from P30DK43351, U01DK062432, R01DK64869, Helmsley grant 2015PG-IBD001 and CCFA. C.A.A. and J.C.B are supported by Wellcome Trust grant 098051. M.G. acknowledges grant support from WELBIO (CAUSIBD), BELSPO (BeMGI), Fédération Wallonie-Bruxelles (ARC IBD@Ulg), and Région Wallonne (CIBLES, FEDER). H.H. acknowledges the ASHG/Charles J. Epstein Trainee Award. J.L. acknowledges Wellcome Trust grant 098759/Z/12/Z. D.M. is supported by the Olle Engkvist Foundation and Swedish Research Council (grants 2010-2976 and 2013-3862). R.K.W. is supported by a VIDI grant (016.136.308) from the Netherlands Organization for Scientific Research (NWO). J.D.R. holds a Canada Research Chair and this work was supported by grants from the U.S. National Institute of Diabetes and Digestive and Kidney Diseases (DK064869; DK062432), a grant (CIHR #GPG-102170) from the Canadian Institutes of Health Research to the "CIHR Emerging Team in Integrative Biology of Inflammatory Diseases", and a *Large-Scale Applied Research Project in Genomics and Personalized Health* grant (GPH-129341) co-funded by the Government of Canada through Genome Canada and the Ministère de l'économie, de l'innovation et de l'exportation du Québec through Génome Québec as well as the Canadian Institutes of Health Research and Crohn's Colitis Canada. J.H.C. is funded by U01 DK62429, U01 DK062422, and the Sanford J. Grossman Charitable Trust. R.H.D. holds the Inflammatory Bowel Disease Genetic Research Chair at the University of Pittsburgh and acknowledges grant support from U01DK062420 and R01CA141743. E.D. benefitted from a Marie-Curie Fellowship and A-S.G a from fellowships from the FNRS and Fonds Léon Fredericq. J.H. is supported by the Örebro University Hospital Research Foundation and the Swedish Research Council (grant no. 521 2011 2764). M.P. acknowledges the NIHR Biomedical Research Centre awards to Guy's & St Thomas' NHS Trust / King's College London and to Addenbrooke's Hospital / University of Cambridge School of Clinical Medicine. D.E.: this work was supported by the German Federal Ministry of Education and Research (BMBF) within the framework of the e:Med research and funding concept (SysInflame grant 01ZX1306A). This project received infrastructure support from the DFG Excellence Cluster No. 306 "Inflammation at Interfaces". A.F. receives an endowment professorship by the Foundation for Experimental Medicine (Zuerich, Switzerland). Additional acknowledgements for the original data are in the Supplementary Information.

Author Contributions Overall project supervision and management: M.J.D. J.C.B, M.G. Fine-mapping algorithms: H.H., M.F., L.J. TFBS analyses: H.H., K.F. Epigenetic analyses: M.U.M., G.T. eQTL dataset generation: E.L., E.T., J.D., E.D., M.E., R.M., M.M., Y.M., V.D., A.G. eQTL analyses: M.F., J.D., L.J., A.C. Variance component analysis: T.M., M.F. Contribution to overall statistical analyses: G.B. Primary drafting of the manuscript: M.J.D., J.C.B, M.G., H.H., L.J. Major contribution to drafting of the manuscript: M.F., M.U.M., J.H.C., D.P.M., J.D.R., C.G.M., R.H.D., R.K.W. The remaining authors contributed to the study conception, design, genotyping QC and/or writing of the manuscript. All authors saw, had the opportunity to comment on, and approved the final draft.

Author Information The authors declare no competing financial interests. Correspondence and requests for materials should be addressed to H.H. (hhuang@atgu.mgh.harvard.edu), M.G. (michel.georges@ulg.ac.be), M.J.D. (mjdaly@atgu.mgh.harvard.edu) or J.C.B. (jb26@sanger.ac.uk)

482 **Table 1.** Summary of variants having posterior probability >50%. Variants were sorted
483 by their posterior probabilities. AF: allele frequency. PROB: posterior probability for
484 being a causal variant. FUNC: functional annotations including coding (C), disrupting
485 transcription factor binding sites (T), Epegenetic peaks (E) and colocalization with eQTL
486 (Q).

VARIANT	CHR	POSITION	TRAIT	AF	PROB	FUNC	ANNOTATION
Signals mapped to a single variant							
rs7307562	12	40724960	CD	0.398	0.999		LRRK2 (intronic)
rs2066844	16	50745926	CD	0.063	0.999	C	NOD2(R702W)
rs2066845	16	50756540	CD	0.022	0.999	C	NOD2(G908R)
rs6017342	20	43065028	UC	0.544	0.999	E	HNF4A (downstream), Gut_H3K27ac
rs61839660	10	6094697	CD	0.094	0.999	E	IL2RA (intronic), Immune_H3K4me1
rs5743293	16	50763781	CD	0.964	0.999	C	fs1007insC
rs6062496	20	62329099	IBD	0.587	0.996	T	RTEL1-TNFRSF6B (ncRNA_intronic), EBF1 TFBS
rs141992399	9	139259592	IBD	0.005	0.995	C	CARD9(1434+1G>C)
rs35667974	2	163124637	UC	0.021	0.994	C	IFIH1(I923V)
rs74465132	7	50304782	IBD	0.034	0.994	T,E	IKZF1 (upstream), EP300 TFBS, Immune_H3K4me1
rs4676408	2	241574401	UC	0.508	0.994		GPR35 (downstream)
rs5743271	16	50744688	CD	0.007	0.993	C	NOD2(N289S)
rs10748781	10	101283330	IBD	0.55	0.990	E	NKX2-3 (upstream), Gut_H3K27ac
rs35874463	15	67457698	IBD	0.054	0.989	C,E	SMAD3(I170V), Gut_H3K27ac
rs72796367	16	50762771	CD	0.023	0.983		NOD2 (intronic)
rs1887428	9	4984530	IBD	0.603	0.974		JAK2 (upstream)
rs41313262	1	67705900	CD	0.014	0.973	C	IL23R(V362I)
rs28701841	6	106530330	CD	0.116	0.971		PRDM1 (upstream)
Signals mapped to 2-50 variants but the lead variant have posterior probability > 50%							
rs76418789	1	67648596	CD	0.006	0.937	C	IL23R(G149R)
rs7711427	5	40414886	CD	0.633	0.919		
rs1736137	21	16806695	CD	0.407	0.879		
rs104895444	16	50746199	CD	0.003	0.865	C	NOD2(V793M)
rs56167332	5	158827769	IBD	0.353	0.845		IL12B
rs104895467	16	50750810	CD	0.002	0.833	C	NOD2(N852S)
rs630923	11	118754353	CD	0.153	0.820		
rs3812565	9	139272502	IBD	0.402	0.815	Q	eQTL of INPP5E in CD4 and CD8; CARD9 in CD14, SEC16A in CD15
rs4655215	1	20137714	UC	0.763	0.784	E	Gut_H3K27ac

rs145530718	19	10568883	CD	0.023	0.762		
rs6426833	1	20171860	UC	0.555	0.752		
chr20: 43258079	20	43258079	CD	0.041	0.736		
rs17229679	2	199560757	UC	0.028	0.716		
rs4728142	7	128573967	UC	0.448	0.664	E	Immune_H3K4me1
rs2143178	22	39660829	IBD	0.157	0.662	T,E	NFKB TFBS, Gut_H3K27ac
rs34536443	19	10463118	CD	0.038	0.649	C	TYK2(P1104A)
rs138425259	16	50663477	UC	0.009	0.648		
rs146029108	9	139329966	CD	0.036	0.643		
rs12722504	10	6089777	CD	0.26	0.615		
rs60542850	19	10488360	IBD	0.17	0.591		
rs2188962	5	131770805	CD	0.44	0.590	E,Q	Gut_H3K27ac, eQTL of SLC22A5 in CD14, CD15 and IL
rs2019262	1	67679990	IBD	0.4	0.586		
rs3024493	1	206943968	IBD	0.171	0.537	E	Immune_H3K4me1
rs7915475	10	64381668	CD	0.304	0.528		
rs77981966	2	43777964	CD	0.077	0.521		
rs9889296	17	32570547	CD	0.264	0.512		
rs2476601	1	114377568	CD	0.908	0.508	C	PTPN22(W620R)

487

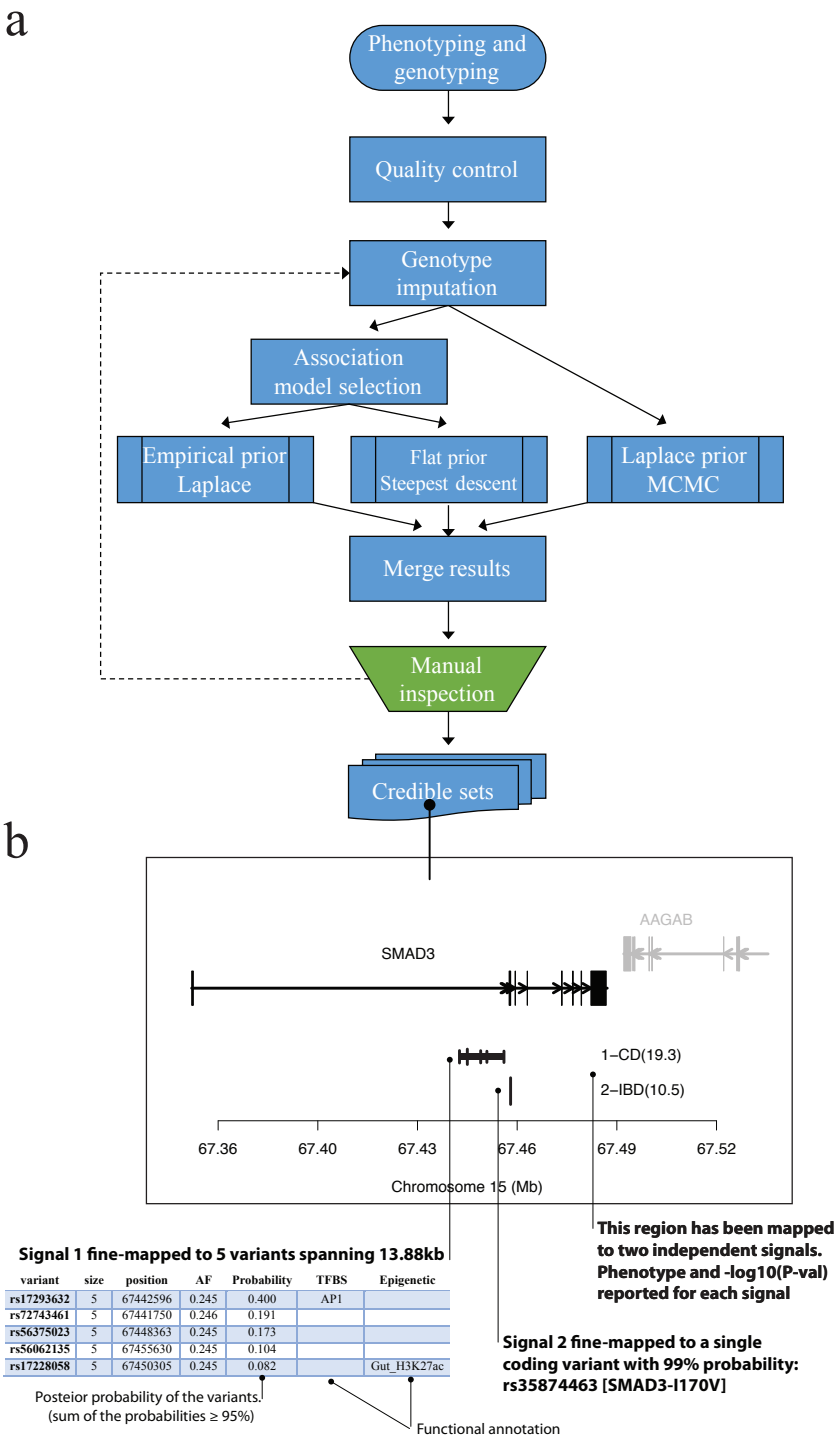

Figure 1. Procedures in the fine-mapping analysis. a, Flowchart of fine-mapping steps. Dashed line means the imputation has been performed only once after manual inspection (not iteratively). **b,** An example output from fine-mapping. This region has been mapped to two independent signals. For each signal, fine-mapping reports the phenotype it is associated with, the variants it is fine-mapped to and their posterior probabilities.

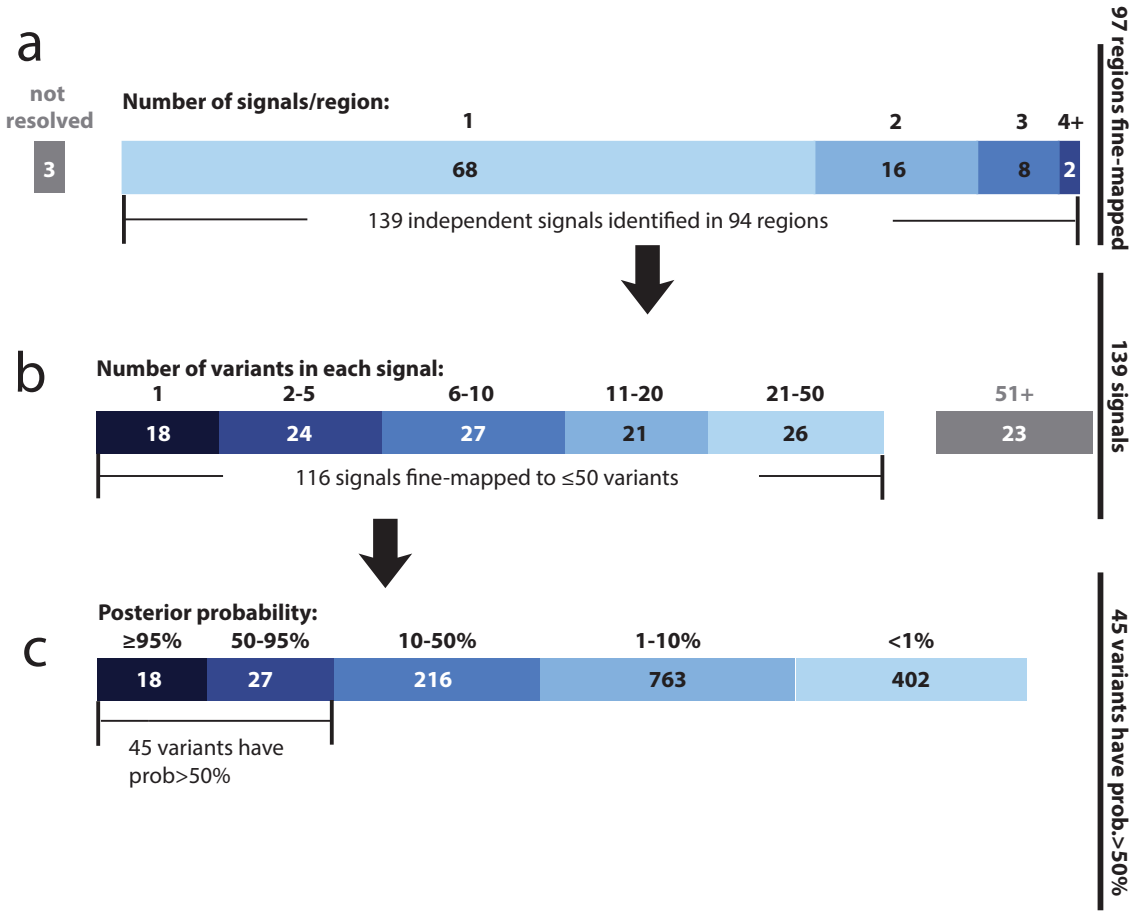

Figure 2. Summary of fine-mapped associations. a, sixty-eight loci hosting a single association and 26 loci hosting multiple independent associations. **b,** Number of variants in credible sets. 18 associations were fine-mapped to a single variant, and 116 to ≤ 50 variants. Only credible sets having ≤ 50 variants were advanced for set-enrichment analyses (epigenetics and eQTL). **c,** distribution of the posterior probability in credible sets having ≤ 50 variants. 45 variants have posterior probability > 50% and were advanced for variant-based enrichment analyses (coding, TFBS disruption and epigenetics).

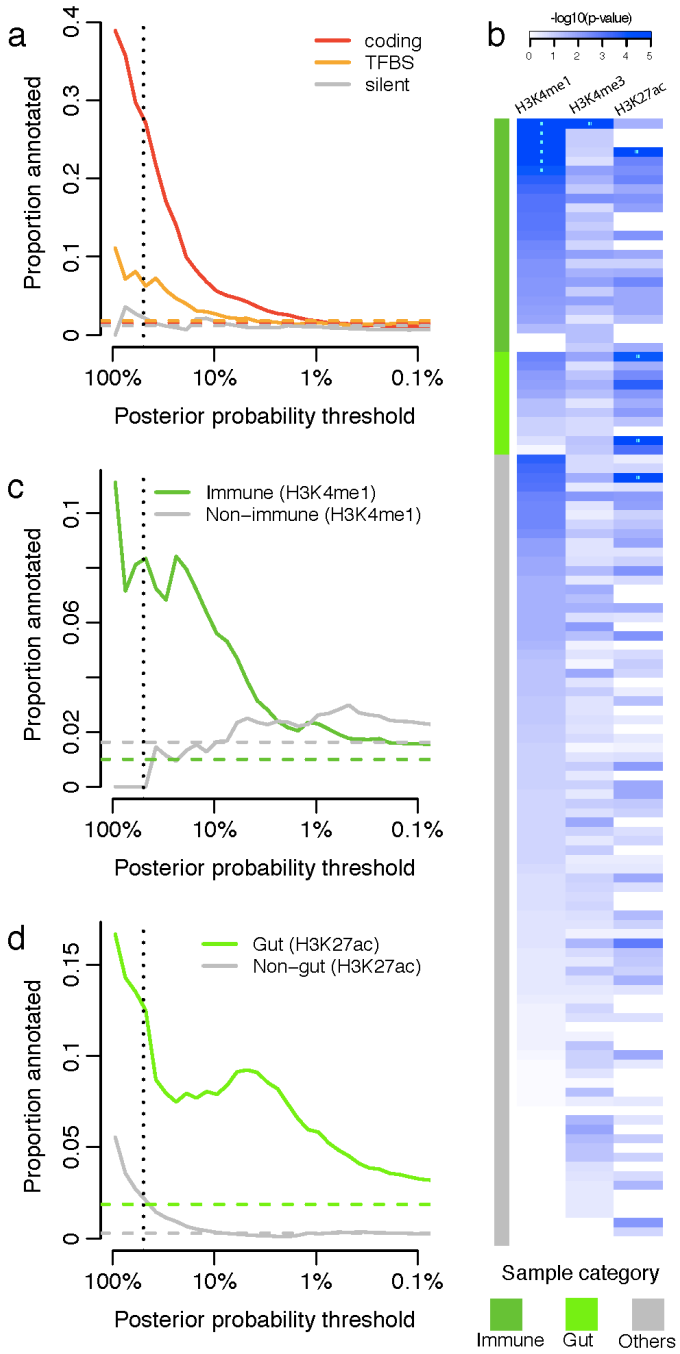

Figure 3. Functional annotation of causal variants. a, Proportion of variants that are protein coding, disrupting/creating transcription factor binding motifs (TFBS) or synonymous. **b,** Epigenetic peaks overlapping credible variants in various cell lines. Sample categories were taken from the Roadmap Epigenomics Consortium[36]. Significant cell line-peak pairs have been marked with asterisks. **c,** Proportion of credible variants that overlap H4K4Me1 peaks. **d,** Proportion of credible variants that overlap H3K27ac peaks. In panels **a**, **c** and **d**, the vertical dotted lines mark the 50% probability and the horizontal dashed lines show the background proportions of each functional category.

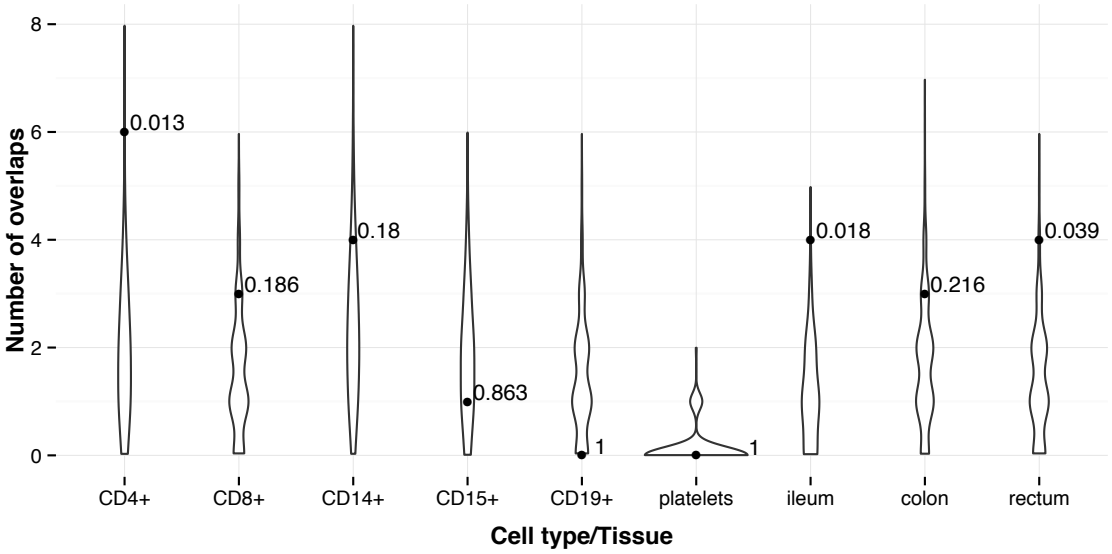

Figure 4. Number of credible sets that colocalize eQTLs. The violin plot shows the distribution of the number of colocalizations by chance (background) and the solid points shows the observed number of colocalizations. P-values of the enrichment were shown next to the solid points. Both the background and the observed numbers were calculated using the permutation based approach (Methods).

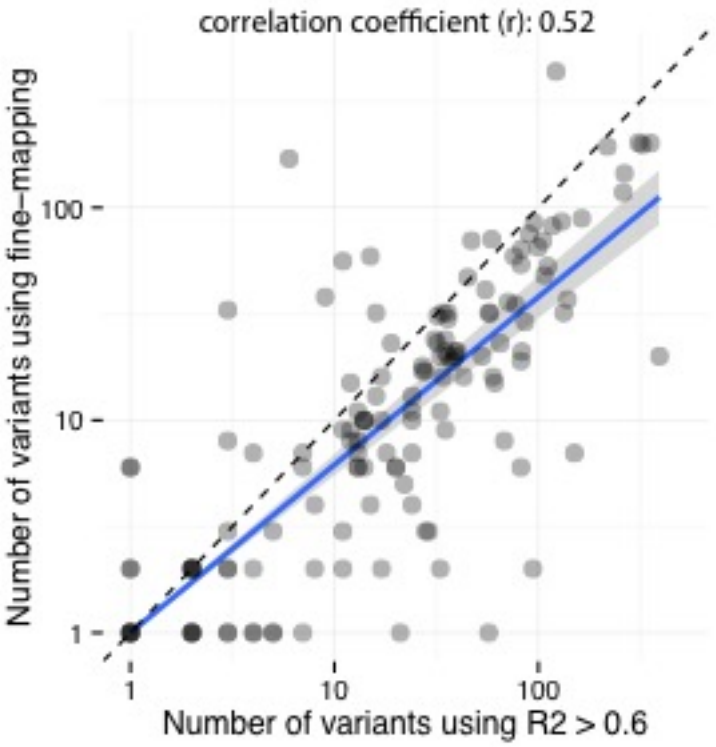

Figure 5. Fine-mapping improved the resolution of genetic associations. We compare the numbers of variants that are mapped in each independent signal using the fine-mapping approach (y axis) and the $R^2 > 0.6$ cut-off (x axis). Fine-mapping maps most signals to smaller numbers of variants.

526 # Methods

527 **Genotyping and QC**

528 We genotyped 35,197 unaffected and 35,346 affected individuals (20,155 Crohn's
529 disease and 15,191 ulcerative colitis) using the Immunochip array. Genotypes were
530 called using optiCall[37] for 192,402 autosomal variants before QC. We removed variants
531 with missing data rate >2% across the whole dataset, or >10% in any one batch, and
532 variants that failed (FDR < 10^{-5} in either the whole dataset or at least two batches) tests
533 for: a) Hardy-Weinberg equilibrium; b) differential missingness between cases and
534 controls; c) significant heterogeneity in allele frequency across controls from different
535 batches. We also removed noncoding variants that were not in the 1000 Genomes Phase I
536 integrated variant set (March 2012 release), or the HapMap phase 2 or 3 releases, as these
537 mostly represent false positives included on Immunochip from the 1000 Genomes pilot,
538 which often genotype poorly. Where a variant failed in exactly one batch we set all
539 genotypes to missing for that batch (to be reimputed later) and included the site if it
540 passed in the remainder of the batches. We removed individuals that had >2% missing
541 data, had significantly higher or lower (defined as FDR<0.01) inbreeding coefficient (*F*),
542 or were duplicated or related (PI_HAT ≥ 0.4, calculated from the LD pruned dataset
543 described below), by sequentially removing the individual with the largest number of
544 related samples until no related samples remain. After QC, there were 67,852 European-
545 derived samples with valid diagnosis (healthy control, Crohn's disease or ulcerative
546 colitis), and 161,681 genotyped variants available for downstream analyses.

547 **Linkage-disequilibrium pruning and principal components analysis**

548 From the clean dataset we removed variants in long range LD[38] or with MAF < 0.05, and
549 then pruned 3 times using the '--indep' option in PLINK (with window size of 50, step
550 size of 5 and VIF threshold of 1.25). This pruned dataset (18,123 variants) was used to
551 calculate the relatedness of the individuals and the principal components. Principal
552 component axes were generated within controls using this LD pruned dataset. The axes
553 were then projected to cases to generate the principal components for all samples. The
554 analysis was performed using our in-house C code
555 (https://github.com/hailianghuang/efficientPCA) and LAPACK package[39] for efficiency.

556 **Imputation**

557 Imputation was performed separately in each Immunochip high-density region (184 total)
558 from the 1000 Genomes Phase I integrated haplotype reference panel, downloaded from
559 the IMPUTE2 website (Dec 2013 release). We used SHAPEIT (v2.r769)[40,41] to pre-phase
560 the genotypes, followed by IMPUTE2 (2.3.0)[14,15] to perform the imputation. There were
561 388,432 variants having good imputation quality (INFO > 0.4) and were used in the fine-
562 mapping analysis.

563 **Manual cluster plot inspection**

564 Variants that had posterior probability greater than 50% or in credible sets mapped to ≤
565 10 variants were manually inspected using Evoker v2.2[42]. Each variant was inspected by
566 3 independent reviewers (10 reviewers participated) and scored as pass, fail or maybe.
567 We remove variants that received one or more fails, or received less than 2 passes. 650
568 out of 905 inspected variants passed this inspection. A further cluster plot inspection
569 flagged two additional failed variants after removing the failed variants from the first
570 inspection and redoing the imputation and analysis.

571 **Establishing a p-value threshold**

572 We used a multiple testing corrected p-value threshold for associations of 10^{-6}, which was
573 established by permutation. We generated 200 permuted datasets by randomly shuffling
574 phenotypes across samples and carried out association analyses for each permutation
575 across all 161,681 variants in our high-density regions. We stored (i) the ensuing
576 161,681 x 200 point-wise p-values (α_S), as well as (ii) the 200 "best" p-values (α_B) of
577 each permuted datasets. We then computed the empirical, family-wise p-value
578 (α_M)(corrected for multiple testing) for each of the 161,681 x 200 tests as its rank/200
579 with respect to the 200 α_B. We then estimated the number of independent tests
580 performed in the studied regions, *n*, as the slope of the regression of log(1-α_M) on log(1-
581 α_S), knowing that $\alpha_M = 1 - (1 - \alpha_S)^n$.

582 **Detecting and fine-mapping association signals**

583 We used three fine-mapping methods to detect independent signals and create credible
584 sets across 103 high-density regions (Supplementary Methods). Signals identified by
585 different methods were merged if their credible sets shared one or more variants. In order
586 to adjudicate differences between methods, we first assigned each candidate signal to the
587 combination of a lead variant and trait (CD, UC or IBD) that maximizes the marginal
588 likelihood from equation (8) in Supplementary Methods. At loci with >1 signal, we fixed
589 the signals reported by all three methods, and then tested all possible combinations of
590 signals reported by one or two methods, selecting whichever combination has the highest
591 joint marginal likelihood. We consider signals to be confidently fine-mapped, and take
592 them forward for subsequent analysis, if they a) are in loci where the lead variant has p <

593 10^{-6}, b) have a ratio of Bayes factors for the best model and the second best model greater
594 than 10, c) are reported by more than one method and d) passed cluster plot inspection.

595 **Phenotype assignment of signals**

596 We assign each signal as CD-specific, UC-specific or shared, using the Bayesian
597 multinomial model used for fine-mapping method 2 (the method best able to assess
598 evidence of sharing in the presence of potentially correlated effect sizes). For the lead
599 variant for each credible set, we calculate the marginal likelihoods as in equation 13 from
600 Supplementary Methods, restricting either $\beta_{UC} = 0$ (for the CD-only model) or $\beta_{CD} =$
601 0 (for the UC-only model), as well as using the unconstrained prior (for the associated to
602 both model), and select the model with the highest marginal likelihood. We then calculate
603 the log Bayes factor in favor of sharing, i.e. the log of ratio of marginal likelihoods
604 between the associated-to-both model and the best of the single-phenotype associated
605 models.

606 **Estimating the variance explained by the fine-mapping**

607 We used a mixed model framework to estimate the total risk variance attributable to the
608 IBD risk loci, and to the signals identified in the fine-mapping. We the GCTA software
609 package[43] to compute a gametic relationship matrix (G-matrix) using genotype dosage
610 information for the genotyped variants in the high-density regions (which we will call
611 $\mathbf{G}_{HD}$). We then fit a variety of variance component models by restricted maximum
612 likelihood analysis using an underlying liability threshold model implemented with the
613 DMU package[44]. The first model is a standard heritability mixed-model that includes
614 fixed effects for five principal components (to correct for stratification) and a random

615 effect summarizing the contribution of all variants in the fine-mapping regions, such that
616 the liabilities across all individuals are distributed according to

617 $$\boldsymbol{L} \sim \boldsymbol{N}(\beta_1 PC_1 + \cdots + \beta_5 PC_5,\ \lambda_1 \mathbf{G}_{HD} + (1 - \lambda_1) I\ ),$$

618 where λ_1 is thus the variance explained by all variants in fine-mapping regions, which
619 we estimate. We then fitted a model that included an additional random effect for the
620 contribution of the lead variants have been specifically identified (with G-matrix
621 $\mathbf{G}_{Signals}$), such that liability is distributed

622 $$\boldsymbol{L} \sim \boldsymbol{N}(\beta_1 PC_1 + \cdots + \beta_5 PC_5,\ \lambda'_1 \mathbf{G}_{HD} + \lambda_2 \mathbf{G}_{Signals} + (1 - \lambda'_1 - \lambda_2) I\ )$$

623 The variance explained by the signals under consideration is then given by the reduction
624 in the variance explained by all variants in the fine-mapping regions between the two
625 models ($\lambda_1 - \lambda'_1$). We used this approach to estimated what fraction of this variance
626 was accounted for by (i) the single strongest signals in each region (as would be typically
627 done prior to fine-mapping), or (ii) the all signals identified in fine-mapping. We used
628 Cox and Snell's method[45] to estimate the variance explained across independent signals
629 (Extended Data Figure 2b) for computational efficiency.

630 **Overlap between transcription factor binding motifs and causal variants**

631 For each motif in the ENCODE TF ChIP-seq data (http://compbio.mit.edu/encode-
632 motifs/, accessed Nov 2014) [20], we calculated the overall information content (IC) as the
633 sum of IC for each position[46], and only considered motifs with overall IC ≥ 14 bits
634 (equivalent to 7 perfectly conserved positions). For every variant in a high-density region
635 we determined if it creates or disrupts a motif at a high-information site (IC ≥ 1.8). For
636 each credible set that contains a motif-affecting variant, we calculated a p-value as 1 −

637 $(1-f)^n$, where n is the size of the credible set and f is the proportion of all variants in
638 the high-density region that disrupt or a create a motif in that TF family.

639 **Overlap between epigenetic signatures and causal variants**

640 For each combination of 120 tissues and three histone marks (H3K4me1, H3K4me3 and
641 H3K27ac) from the Roadmap Epigenome Project we calculated an overlap score, equal
642 to the sum of fine-mapping posterior probabilities for all variants in peaks of that histone
643 mark in that tissue. We generated a null distribution of this score for each tissue/mark by
644 shifting chromatin marks randomly over the high-density regions (shifting the peaks
645 from their actual position by a random number of bases while keeping inter-peak spacing
646 the same) and calculating the overlap score for each permutation. To summarize these
647 correlated results across many cell and tissue types we defined a set of "core" H3K4me1
648 immune and H3K27ac gut peaks as sets of overlapping peaks in cells that showed the
649 strongest enrichment ($p<10^{-4}$). Intersects were made using bedtools v2.24.0 default
650 settings[47]. We selected 6 immune cell types for H3K4me1 and 3 gut cell types for
651 H3K27ac (Supplementary Table 2). We also chose controls (Supplementary Table 2)
652 from non-immune and non-gut cell types with similar density of peaks in the fine-
653 mapped regions as compared to immune/gut cell types to confirm the tissue-specificity of
654 the overlap. We used the phenotype assignments (described above) in dissecting the
655 enrichment for the CD and UC signals. Sixty-five CD and 21 UC signals were used in
656 this analysis.

657 **Published eQTL summary statistics**

658 We used eQTL summary statistics from two published studies:

659 • Peripheral blood eQTLs from the GODOT study[48] of 2,752 twins, reporting loci with
660 MAF>0.5%.
661 • CD14+ monocyte eQTLs from Table S2 in Fairfax *et al.*[31], comprised of 432
662 European individuals, measured in a naïve state and after stimulation with interferon-
663 γ (for 2 or 24 hours) or lipopolysaccharide. Reports loci with MAF>4% and
664 FDR<0.05.

665 **Processing and quality control of new eQTL ULg dataset**

666 A detailed description of the ULg dataset is in preparation (Momozawa et al., in
667 preparation). Briefly, we collected venous blood and intestinal biopsies at three locations
668 (ileum, transverse colon and rectum) from 350 healthy individuals of European descent,
669 average age 54 (range 17-87), 56% female. SNPs were genotyped on Illumina Human
670 OmniExpress v1.0 arrays interrogating 730,525 variants, and SNPs and individuals were
671 subject to standard QC procedures using call rate, Hardy-Weinberg equilibrium, MAF ≥
672 0.05, and consistency between declared and genotype-based sex as criteria. We further
673 imputed genotypes at ~7 million variants on the entire cohort using the Impute2 software
674 package[14] and the 1,000 Genomes Project as reference population (Phase 3 integrated
675 variant set, released 12 Oct 2014) [11,15]. From the blood, we purified CD4+, CD8+,
676 CD19+, CD14+ and CD15+ cells by positive selection, and platelets (CD45-negative) by
677 negative selection. RNA from all leucocyte samples and intestinal biopsies was
678 hybridized on Illumina Human HT-12 arrays v4. After standard QC, raw fluorescent
679 intensities were variance stabilized[49] and quantile normalized[50] using the lumi R
680 package[51], and were corrected for sex, age, smoking status, number of probes with
681 expression level significantly above background as fixed effects and array number

682 (sentrix id) as random effect. For each probe with measureable expression (detection p-
683 value < 0.05 in >25% of samples) we tested for cis-eQTLs at all variants within a 500
684 kilobase window. The nominal p-value of the best SNP within a cis-window was Sidak-
685 corrected for the window-specific number of independent tests, and we estimated false
686 discovery rates (q-values) from the resulting p-values across all probes using the qvalue
687 R package[52]. 480 cis-eQTL with FDR ≤ 0.10 with the lead SNPs within the 97 high-
688 density regions (94 fine-mapped plus 3 unresolved) were retained for further analyses.

689 **Naïve co-localization using lead SNPs**

690 We calculated the proportion of IBD credible sets that contain a lead eQTL variant in a
691 particular tissue. This value is then compared to a background rate:

692 $$\frac{1}{|S|}\sum_{i\in S}(1-(1-N_i^{-1})^{C_i})$$

693 where N_i is the total number of variants in region i in 1000 Genomes with an allele
694 frequency greater than a certain threshold (equal to the threshold used for the original
695 eQTL study), C_i is the number of these variants that lie in IBD credible sets, and S is a set
696 of regions that have at least one significant eQTL ($|S|$ is the number of regions in this
697 set). P-values can then be calculated assuming a binomial distribution with probability
698 equal to the background rate and the number of trials equal to $|S|$.

699 **Frequentist co-localization using conditional p-values**

700 We next used conditional association to test for evidence of co-localization, as described
701 in Nica et al.[25]. This method compares the p-value of association for the lead SNP of an
702 eQTL before and after conditioning on the SNP with the highest posterior in the credible
703 set, and measures the drop in log(1/p). An empirical p-value for this drop is then
704 calculated by comparing it to the drop for all variants (with MAF ≥ 0.05) in the high-

705 density region. An empirical p-value ≤ 0.05 was considered as evidence that the
706 corresponding credible set is co-localized with the corresponding cis-eQTL. To evaluate
707 whether our 139 credible sets affected cis-eQTL more often than expected by chance we
708 counted the number of credible sets affecting at least one cis-eQTL with p-value ≤ 0.05,
709 and compared how often this number was matched or exceeded by 1,000 sets of 139 lead
710 variants that were randomly selected yet distributed amongst the 94 loci in accordance
711 with the real credible sets.

712 **Bayesian co-localization using Bayes factors**

713 Finally, we used the Bayesian co-localization methodology described by Giambartolomei
714 et al[53], modified to use the credible sets and posteriors generated by our fine-mapping
715 methods. The method takes as input a pair of IBD and eQTL signals, with corresponding
716 credible sets S^{IBD} and S^{eQTL}, and posteriors for each variant p_i^{IBD} and p_i^{eQTL} (with
717 $p_i^X = 0 \; \forall \; i \; \notin S^X$). Credible sets and posteriors were generated for eQTL signals using
718 the Bayesian quantitative association mode in SNPTest (with default parameters), with
719 credible sets in regions with multiple independent signals generated conditional on all
720 other signals. Our method calculates a Bayes factor summarizing the evidence in favor of
721 a colocalized model (i.e. a single underlying causal variant between the IBD and eQTL
722 signals) compared to a non-colocalized model (where different causal variants are driving
723 the two signals), given by the ratio of marginal likelihoods

724 $$BF = \frac{L(Colocalized)}{L(Not\ colocalized)}.$$

725 The marginal likelihood for the colocalized model (i.e. hypothesis H_4 in Giambartolomei
726 et al) is given by

$$L(Colocalized) \propto \frac{1}{N} \sum_{i \in S^{IBD} \cup S^{eQTL}} p_i^{IBD} p_i^{eQTL}$$

and the likelihood for the model where the signals are not colocalized (i.e., hypothesis H_3) is given by:

$$L(Not\ colocalized) \propto \frac{1}{N^2 - N} \sum_{i,j \in S^{IBD} \cap S^{eQTL}, i \neq j} p_i^{IBD} p_j^{eQTL}$$

In both cases, N is the total number of variants in the region. We only count towards N variants that have $r^2 > 0.2$ with either the lead eQTL variant or the lead IBD variant.

Permutation analysis. To measure enrichment in colocalization Bayes factors compared to the null, we carried out a permutation analysis. In this analysis, we randomly reassigned eQTL signals to new fine-mapping regions to generate a set of simulated null datasets. This is carried out using the following scheme:

1. Estimate the standarized effect size β_g for each eQTL signal g, equal to standard deviation increase in gene expression for each dose of the minor allele.
2. Randomly reassign each eQTL signal to a new fine-mapping region, and then select a new causal variant with a minor allele frequency within 1 percentage point of the lead variant from the real signal. If multiple such variants exist, select one at random. If no such variants exist, pick the variant with the closest minor allele frequency.
3. Generate new simulated gene expression signals for each individual from Normal($\beta_g x_j, 1 - \beta_g^2$) where x_j is the individual's minor allele dosage at the new causal variant and f is the minor allele frequency.
4. Carry out fine-mapping and calculate colocalization Bayes factors for each pair of (real) IBD signal and (simulated) eQTL signal.
5. Repeat stages 2-4 1000 times for each tissue type

749 We can use these permuted Bayes factors to calculate p-values for each IBD credible set,
750 given by the proportion of time the permuted BFs were as large or greater than the one
751 observed in the real dataset. To generate a high-quality set of colocalized eQTL and IBD
752 signals, we take all signals that have BF > 2, p < 0.01 and r^2 between hits of >0.8.
753
754 **References**

755 37. Shah, T. S. *et al.* optiCall: a robust genotype-calling algorithm for rare, low-
756 frequency and common variants. *Bioinformatics* **28,** 1598–1603 (2012).
757 38. Price, A. L. *et al.* Long-Range LD Can Confound Genome Scans in Admixed
758 Populations. *Am J Hum Genet* **83,** 132–135 (2008).
759 39. Anderson, E. *et al. LAPACK Users' Guide*. (Society for Industrial and Applied
760 Mathematics, 1999).
761 40. Delaneau, O., Marchini, J. & Zagury, J.-F. A linear complexity phasing method for
762 thousands of genomes. *Nature Methods* **9,** 179–181 (2011).
763 41. Delaneau, O., Zagury, J.-F. & Marchini, J. Improved whole-chromosome phasing
764 for disease and population genetic studies. *Nature Methods* **10,** 5–6 (2012).
765 42. Morris, J. A., Randall, J. C., Maller, J. B. & Barrett, J. C. Evoker: a visualization
766 tool for genotype intensity data. *Bioinformatics* **26,** 1786–1787 (2010).
767 43. Yang, J., Lee, S. H., Goddard, M. E. & Visscher, P. M. GCTA: A Tool for
768 Genome-wide Complex Trait Analysis. *The American Journal of Human Genetics*
769 **88,** 76–82 (2011).
770 44. Madsen, P., Su, G., Labouriau, R. & Christensen, F. DMU-a package for analyzing
771 multivariate mixed models. *Proceedings of the Ninth World Congress on Genetics*
772 *Applied to Livestock Production* (2010).
773 45. Cox, D. R. & Snell, E. J. *Analysis of Binary Data, Second Edition*. (CRC Press,
774 1989).
775 46. D'haeseleer, P. What are DNA sequence motifs? *Nat Biotechnol* **24,** 423–425
776 (2006).
777 47. Quinlan, A. R. & Hall, I. M. BEDTools: a flexible suite of utilities for comparing
778 genomic features. *Bioinformatics* **26,** 841–842 (2010).
779 48. Wright, F. A. *et al.* Heritability and genomics of gene expression in peripheral
780 blood. *Nat Genet* **46,** 430–437 (2014).
781 49. Lin, S. M., Du, P., Huber, W. & Kibbe, W. A. Model-based variance-stabilizing
782 transformation for Illumina microarray data. *Nucleic Acids Res* **36,** e11–e11
783 (2008).
784 50. Bolstad, B. M., Irizarry, R. A., Astrand, M. & Speed, T. P. A comparison of
785 normalization methods for high density oligonucleotide array data based on
786 variance and bias. *Bioinformatics* **19,** 185–193 (2003).
787 51. Du, P., Kibbe, W. A. & Lin, S. M. lumi: a pipeline for processing Illumina
788 microarray. *Bioinformatics* **24,** 1547–1548 (2008).
789 52. Dabney, A., Storey, J. D. & Warnes, G. Q-value estimation for false discovery rate
790 control. *R package version* **1,** (2006).
791 53. Giambartolomei, C. *et al.* Bayesian test for colocalisation between pairs of genetic
792 association studies using summary statistics. *PLoS Genet* **10,** e1004383 (2014).

793

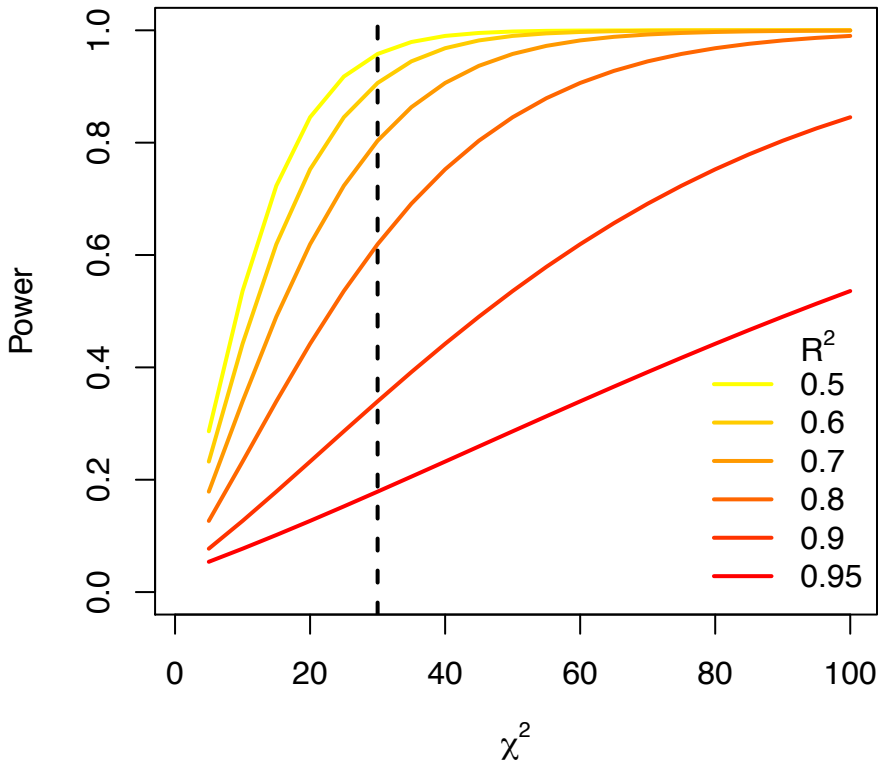

Extended Data Figure 1. Power (y axis) to distinguish which variant in a correlated pair (strength of correlation shown by color) is causal increases with the significance of the association (x axis), and therefore with sample size and effect size. The vertical dashed line flags the genome-wide significance level. To estimate the relationship between the strength of association and our ability to fine-map it, we assumed that the association has only two possible causal variants, and we define the signal as successfully fine-mapped if the ratio of Bayes factors between the true causal variant and the non-causal variant is greater than 10 (a 91% posterior, assuming equal priors). Using equation (8) in Supplementary Methods, we have

$$\text{logBF} = \log\frac{\Pr(\boldsymbol{Y}\,|\text{SNP1})}{\Pr(\boldsymbol{Y}\,|\text{SNP2})} \approx \log\frac{\Pr(\boldsymbol{Y}\,|\text{SNP1},\theta_1^*)}{\Pr(\boldsymbol{Y}\,|\text{SNP2},\theta_2^*)}$$

in which θ^* is maximum likelihood estimate of the parameter values. The log-likelihood ratio follows a chi-square distribution:

$$\text{logBF} \sim -\frac{1}{2}(\chi^2_{\text{SNP1}} - \chi^2_{\text{SNP2}}) = -\frac{1}{2}\lambda(1-r^2)$$

in which λ is the chi-square statistic of the lead variant and *r* is the correlation coefficient between the two variants. Because of the additive property of the chi-square distribution, logBF follows a non-central chi-square distribution with 1 degree of freedom and non-centrality parameter $\lambda(1-r^2)/2$. Therefore, the power can calculated as the probability that logBF > log(10), given by the CDF of the non-central chi-squared distribution.

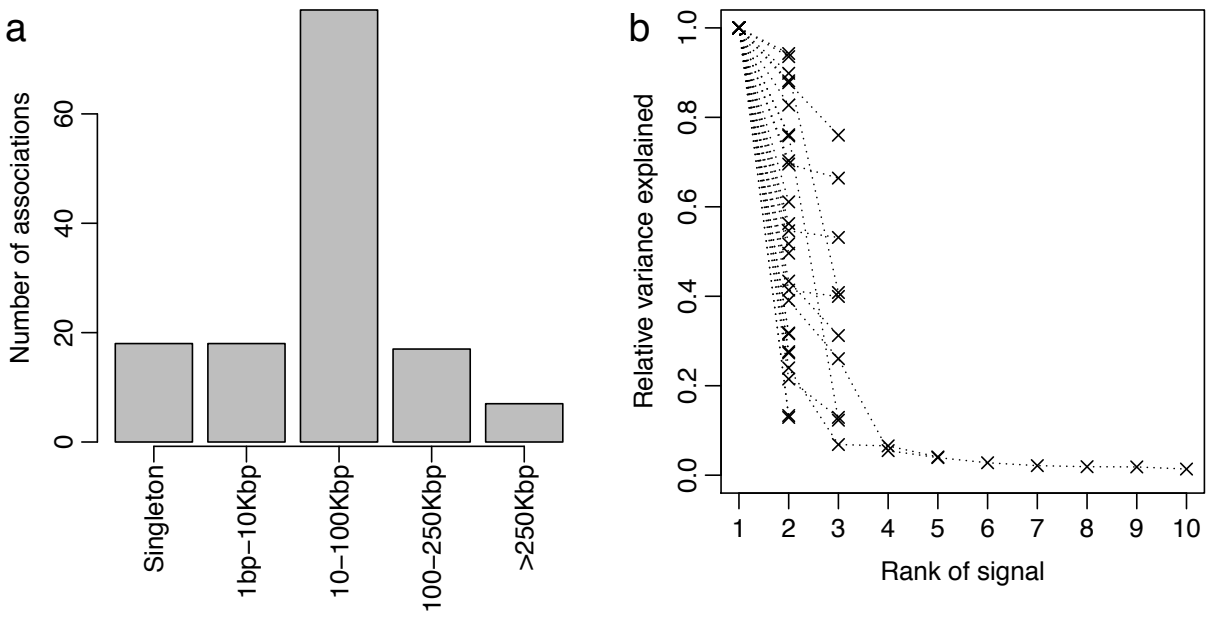

Extended Data Figure 2. a, Genomic distance that variants in 95% credible set span. **b,** Variance explained normalized to the primary association in each locus.

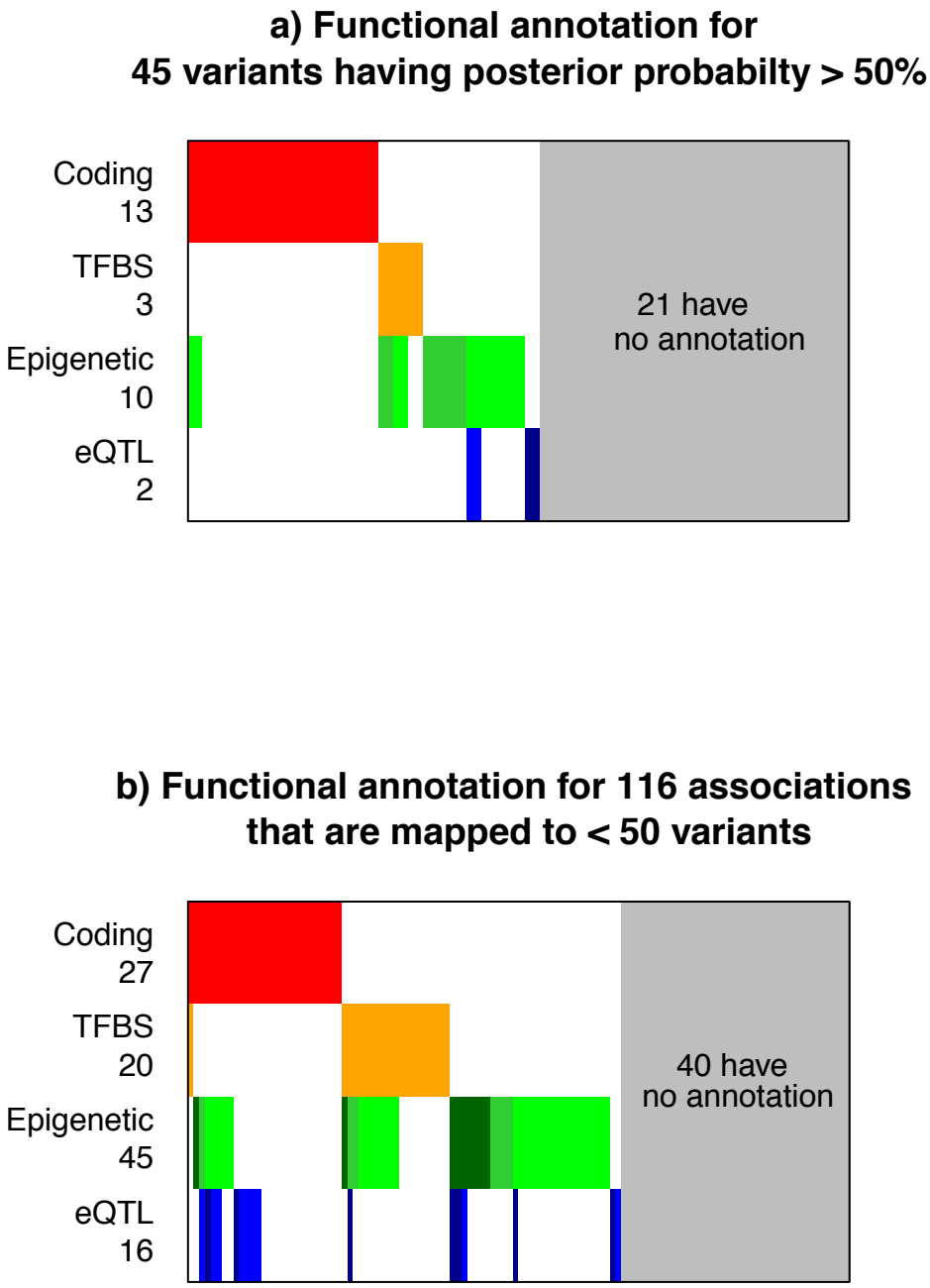

Extended Data Figure 3. a, Functional annotation for 45 variants having posterior probability > 50%. **b,** Functional annotation for 116 associations that are fine-mapped to ≤ 50 variants.

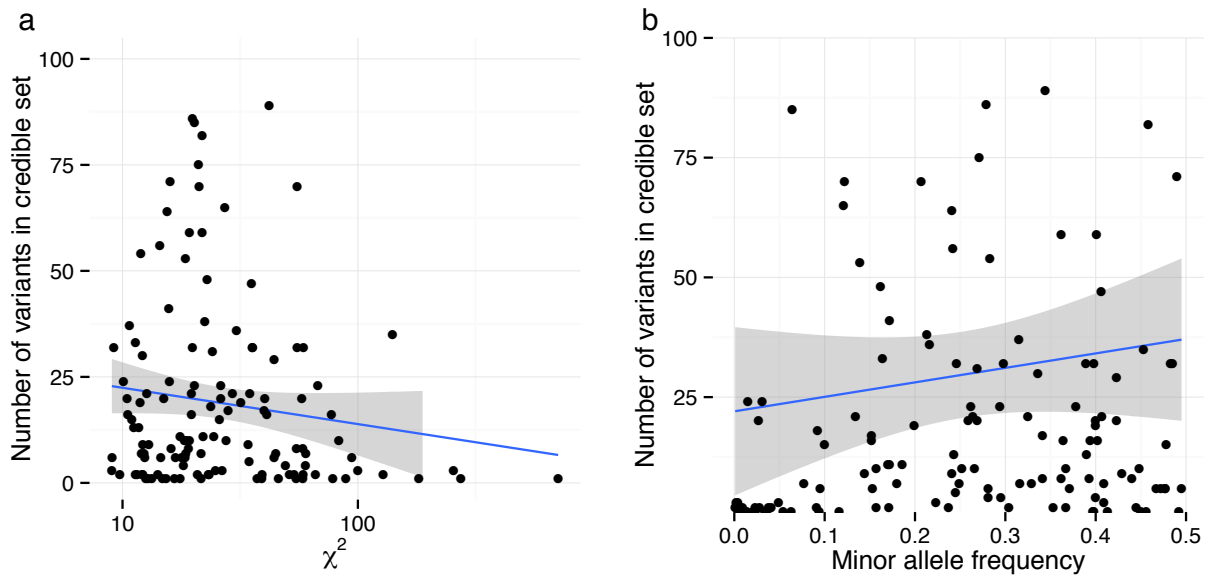

Extended Data Figure 4. **a,** Number of variants in credible set decreases with the significance of the signal. **b,** Number of variants in credible set increases with the minor allele frequency of the signal. The solid line shows the fitted trend in both panels, and the shaded region shows the variance of the trend.

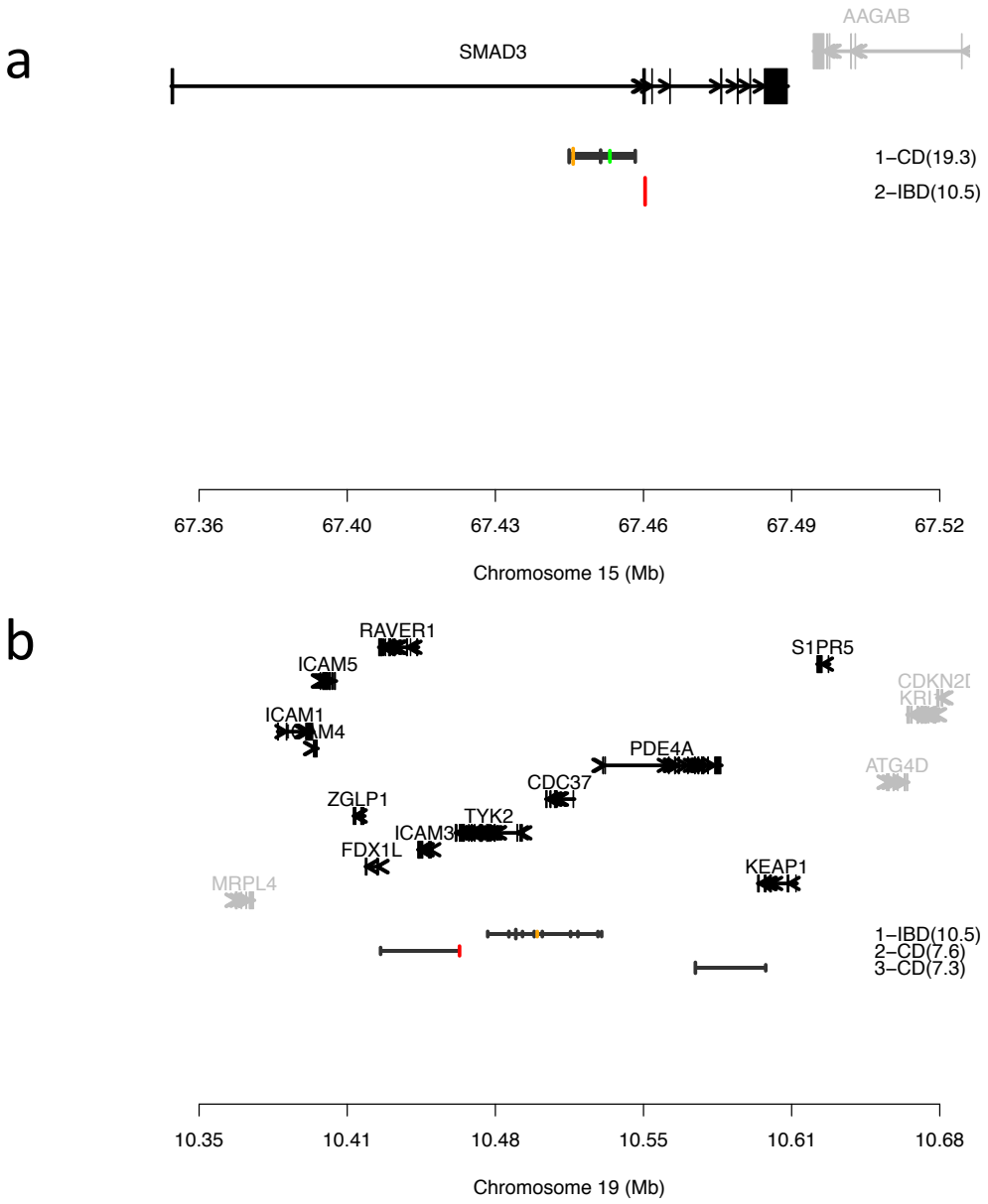

Extended Data Figure 5. SMAD3 (**a**) and TYK2 (**b**) regions after fine-mapping. The implicated region has been reduced to a smaller number of genes (shown in black). Color ticks are variants mapped to their functions (red: non-synonymous, orange: disrupting TFBS, green: overlapping epigenetic marks) and black ticks are variants not mapped to a function. The width of the tick scales with the posterior probability.

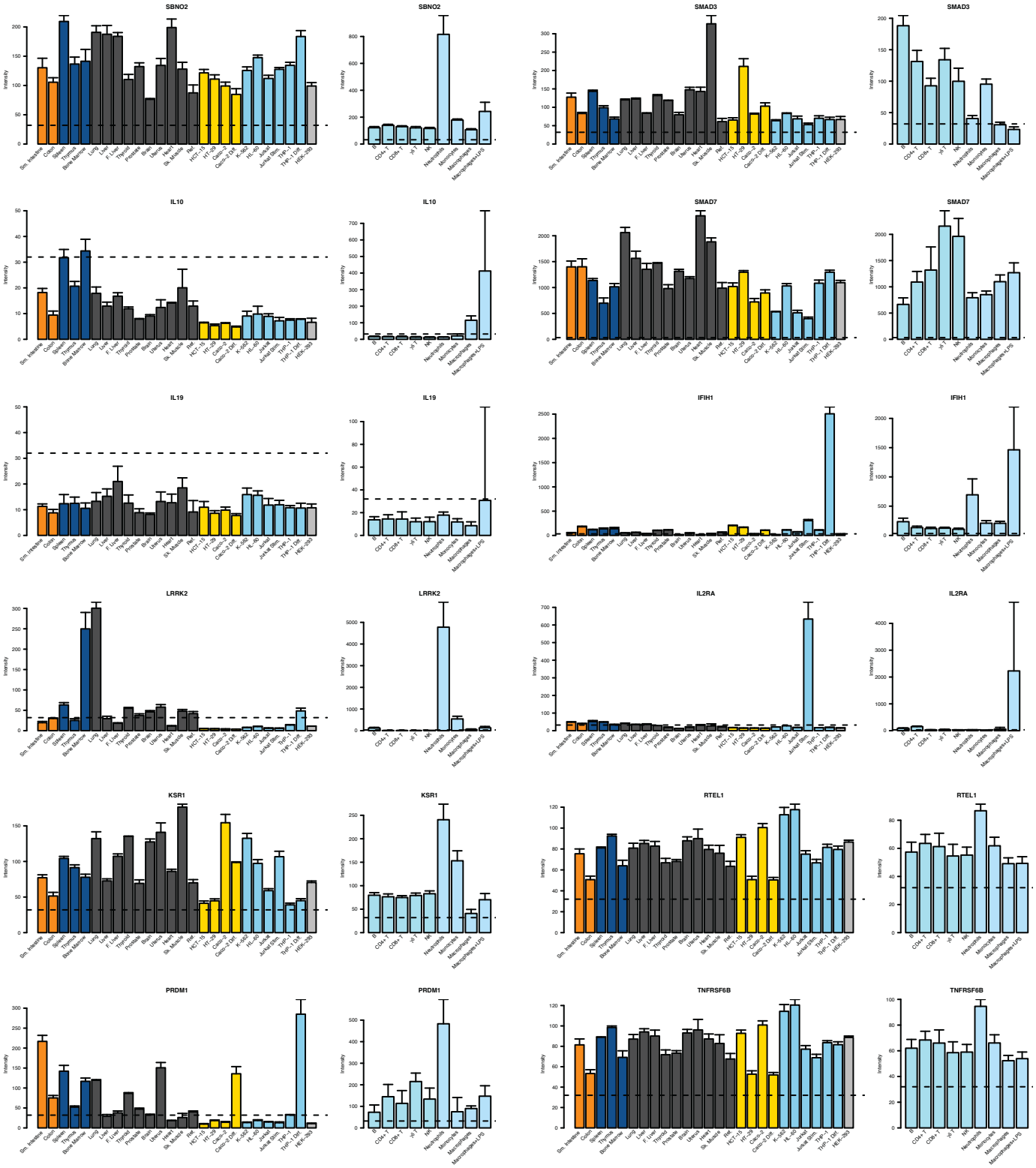
SBNO2
SMAD3
IL10
SMAD7
IL19
IFIH1
LRRK2
IL2RA
KSR1
RTEL1
PRDM1
TNFRSF6B
Intensity
Sm. Intestine
Colon
Spleen
Thymus
Bone Marrow
Lung
Liver
F. Liver
Thyroid
Prostate
Brain
Uterus
Heart
Sk. Muscle
Pancreas
HCT-15
HT-29
Caco-2
Caco-2 Diff.
K-562
HL-60
Jurkat
Jurkat Stim.
THP-1
THP-1 Diff.
HEK-293
B
CD4+ T
CD8+ T
γδ T
NK
Neutrophils
Monocytes
Macrophages
Macrophages+LPS

Extended Data Figure 6. Tissue and cell line specific expression for genes *SBNO2*, *IL10*, *IL19*, *LRRK2*, *KSR1*, *PRDM1*, *SMAD3*, *SMAD7*, *IFIH1*, *IL2RA*, *RETL1* and *TNFRSF6B*. **Left panels.** Expression levels of selected genes were determined in a panel of human tissues (bone marrow, heart, skeletal muscle (Sk. Muscle), uterus, liver, fetal liver (F. Liver), spleen, thymus, thyroid, prostate, brain, lung, small intestine (Sm. Intestine) and colon) and human cell lines using a custom made Agilent expression array. The cell lines represent models of human T lymphocytes (Jurkat), monocytes (THP-1), erythroleukemia cells (K562), promyelocytic cells (HL-60), colonic epithelial cells (HCT-15, HT-29, Caco-2), and cells from embryonic kidney (HEK-293). In addition, models of differentiated colonic epithelium (Caco-2 differentiated for 21 days in culture (Caco-2 diff.)), activated T lymphocytes (Jurkat cells stimulated with PMA (40ng/ml) and ionomycin (1ug/ml) for 6 hrs (Jurkat stim.)), and macrophages (derived from THP-1 differentiated for 24 hrs (THP-1 diff.) with IFN-γ (400U/ml) and TNF-α (10ng/ml)) were examined. Intensity values for each tissue/cell line represent the geometric mean with geometric standard deviation of 3 independent measurements; each measurement represents the geometric mean of all probes (one per exon) for each gene followed by a median normalization across all genes on the array. The dotted line indicates the threshold level for detection of basal expression. The reference sample (Ref.) is composed of a mixture RNAs derived from 10 different human tissues. **Right panels.** Expression levels of selected genes were determined in a panel of primary immune cells (neutrophils, monocytes, γδ T cells, B cells, NK cells, $CD4^+$ T cells, $CD8^+$ T cells) isolated from healthy donors, as well as monocyte *in vitro* derived macrophages without and with 24 hours of stimulation using 1 ug/ml of lipopolysaccharide (macrophages+LPS). The results presented in the **left and right panels** were generated and analyzed separately and therefore the expression values are not directly comparable.

DATASET	METHOD	OBSERVED	EXPECTED	P-VALUE
CD4	**Naïve**	**3**	**0.4**	**0.007**
CD8	Naïve	1	0.3	0.296
CD14	Naïve	0	0.2	1.000
CD15	Naïve	1	0.2	0.199
CD19	Naïve	0	0.1	1.000
Platelets	Naïve	0	0.0	1.000
Ileum	**Naïve**	**2**	**0.3**	**0.025**
Colon	Naïve	1	0.2	0.206
Rectum	Naïve	1	0.2	0.187
CD14 naïve	**Naïve**	**8**	**2.7**	**0.005**
CD14 IFN stimulated	Naïve	4	3.2	0.559
CD14 LPS 2h stimulated	Naïve	1	2.1	0.726
CD14 LPS 24h stimulated	Naïve	5	2.5	0.107
CD4	**Bayesian**	**4**	**1.0**	**0.010**
CD8	Bayesian	1	0.8	0.566
CD14	Bayesian	1	0.9	0.595
CD15	Bayesian	0	0.7	1.000
CD19	Bayesian	0	0.6	1.000
Platelets	Bayesian	0	0.1	1.000
Ileum	Bayesian	2	0.4	0.069
Colon	**Bayesian**	**3**	**0.8**	**0.040**
Rectum	Bayesian	2	0.6	0.124
CD4	**Permutation**	**6**	**1.9**	**0.013**
CD8	Permutation	3	1.5	0.186
CD14	Permutation	4	2.3	0.180
CD15	Permutation	1	1.8	0.863
CD19	Permutation	0	1.4	1.000
Platelets	Permutation	0	0.1	1.000
Ileum	**Permutation**	**4**	**1.1**	**0.018**
Colon	Permutation	3	1.7	0.216
Rectum	**Permutation**	**4**	**1.4**	**0.039**

Extended Data Table 1. The number IBD credible sets that colocalize with expression QTLs using the naïve, permutation-based and Bayesian-based approaches.